Скопления галактик в присутствии темной Energy

G.S.Bisnovatyi-Kogan
Space Research Institute, Moscow

XII Зимняя Школа «Малочастичные системы:
теория и приложения
Дубна, ОИЯИ, 06 февраля 2014 года

Expanding Universe (Friedmann, Lemaitre, Hubble)

Uniform isotropic universe, Einstein equation

$$\frac{\dot{a}^2}{a^2} + \frac{k\,c^2}{a^2} = \frac{8\pi G}{3c^2}\varepsilon + \frac{\Lambda}{3}c^2.$$

Adiabatic expansion:

Для адиабатического расширения имеем

$$\frac{d\varepsilon}{\varepsilon + P} = -\frac{dV}{V} = -3\frac{da}{a}, \qquad \text{V - объем.}$$

Flat universe, k=0, unfinite universe, ***a*** – scale factor

$$\frac{\dot{a}^2}{a^2} = \frac{8\pi G}{3c^2}\varepsilon + \frac{\Lambda}{3}c^2, \quad \varepsilon = \rho c^2 = \rho_* c^2 \frac{a_*^4}{a^4}. \qquad \frac{dx}{dt} = 2\sqrt{\frac{8\pi G\rho_*}{3}a_*^4 + \frac{\Lambda}{3}c^2x^2},$$

$$x = a^2 \qquad a^2 = a_*^2\sqrt{\frac{8\pi G\rho_*}{\Lambda c^2}}\,\mathrm{sh}\left(2\sqrt{\frac{\Lambda}{3}}ct\right).$$

Small **t** - beginning:

$$a^2 = a_*^2\sqrt{\frac{32\pi}{3}G\rho_* t}, \quad \rho = \frac{3}{32\pi G t^2}.$$

Large **t –** exponential expansion at non-zero cosmological constant:

$$a^2 = \frac{a_*^2}{2}\sqrt{\frac{8\pi G\rho_*}{\Lambda c^4}}\exp\left(2\sqrt{\frac{\Lambda}{3}}ct\right), \quad \rho = \frac{\Lambda c^4}{2\pi G}\exp\left(-4\sqrt{\frac{\Lambda}{3}}ct\right).$$

Hot Universe (Gamow, Penzias and Wilson)

Inflation

Early stages:

Exponential expansion (large Lambda term, “excited vacuum”, scalar field),

Inflation – decay of the “excited vacuum” or scalar field,

Stage of Friedmann expansion.

Non-zero Lambda term (much smaller), transition from Friedmann expansion to exponential expansion stage.

For discovery of the expansion law of the present universe we need independent measurements of the velocity and distance to very remote objects (galaxies, quasars, galaxy clusters)

Supernovae Ia – thermonuclear explosion SN – are used for these purposes, due to possibility to find its total luminosity by measurements of its light curve (type of a standard candle)

SN Ia

Composite X-ray and infrared image of the SN 1572 (Tycho's SN) remnant as seen by Chandra X-Ray Observatory, Spitzer Space Telescope, and Calar Alto Observatory

SN Ia

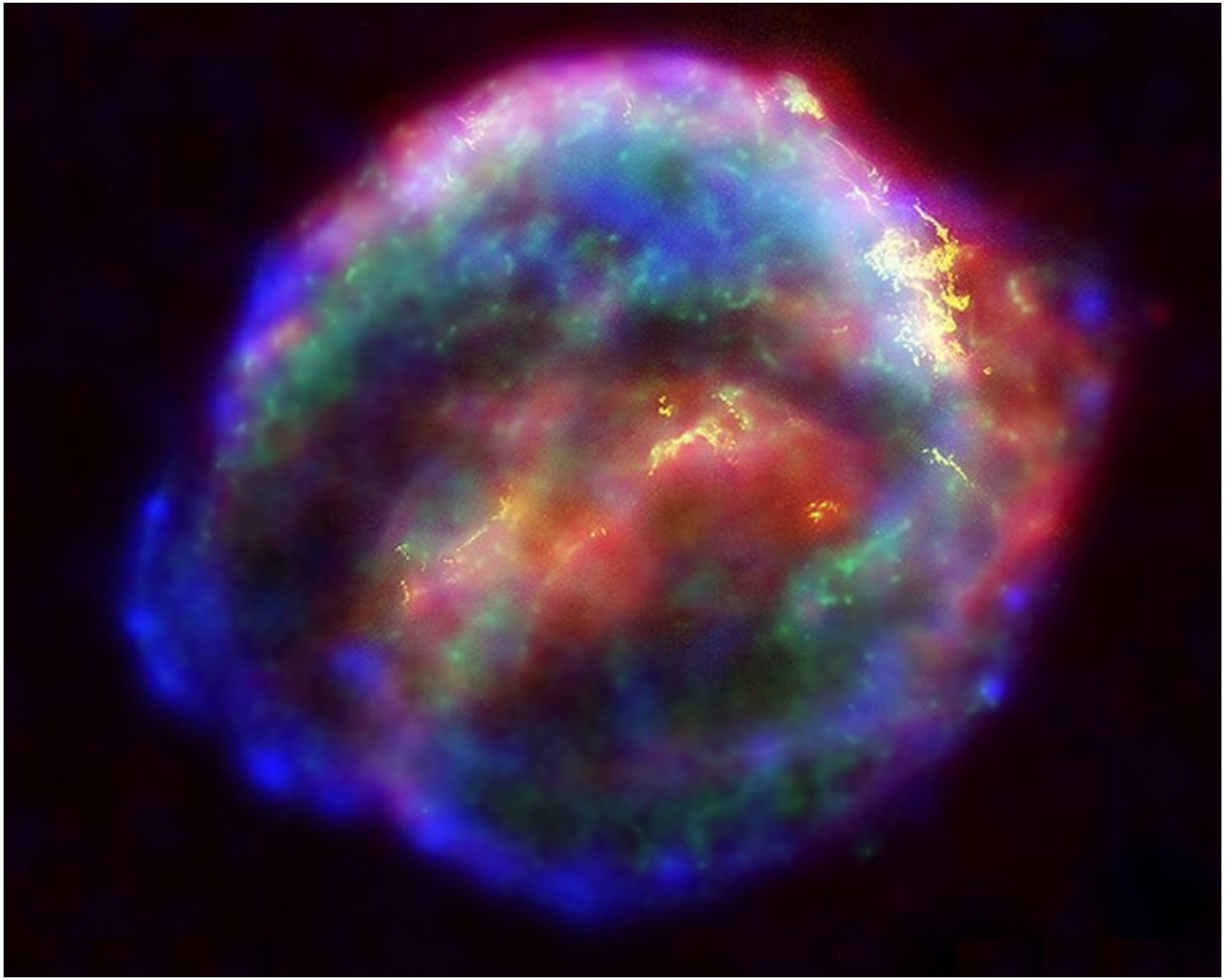

A false-color composite (HST/SIRTF) image of the supernova remnant nebula from SN 1604 (Kepler SN).

SN Ia,

Riess, A. G. + 19 authors

Observational Evidence from Supernovae for an Accelerating Universe and a Cosmological Constant (10 SNIa, 0.16 <= z <= 0.62)

The Astronomical Journal, Vol. 116, Issue 3, pp. 1009-1038 (1998)

Schmidt, B. P. + 23 authors

The Astrophysical Journal, Vol. 507: pp.46-63, 1998 November 1

The High-Z Supernova Search: Measuring Cosmic Deceleration and Global Curvature of the Universe Using Type IA Supernovae

(>30 SNIa, 0.35 <= z <= 0.9)

Omega_M=0.4^+0.5_-0.4, Omega_Lambda=0.6^+0.4_-0.5

Unless supernovae are much different at high redshifts, the imperfection of SNe Ia as distance indicators will have a negligible impact on using SNe Ia as cosmological probes.

Perlmutter, S. + 23 authors (The Supernova Cosmology Project)

Measurements of the Cosmological Parameters Omega and Lambda from the First Seven Supernovae at Z >= 0.35

Astrophysical Journal v.483, pp.565-581 (1997)

For a spatially flat universe (Omega M + Omega Lamda = 1), we find Omega_{M}=0.94^{+0.34}_{-0.28} or, equivalently, a measurement of the cosmological constant, Omega _{ Lamda }=0.06^{+0.28}_{-0.34}

Perlmutter, S. + 32 authors (The Supernova Cosmology Project)

Measurements of Omega and Lambda from 42 High-Redshift Suprnovae (redshifts between 0.18 and 0.83)

The Astrophysical Journal, Volume 517, Issue 2, pp. 565-586 (1999)

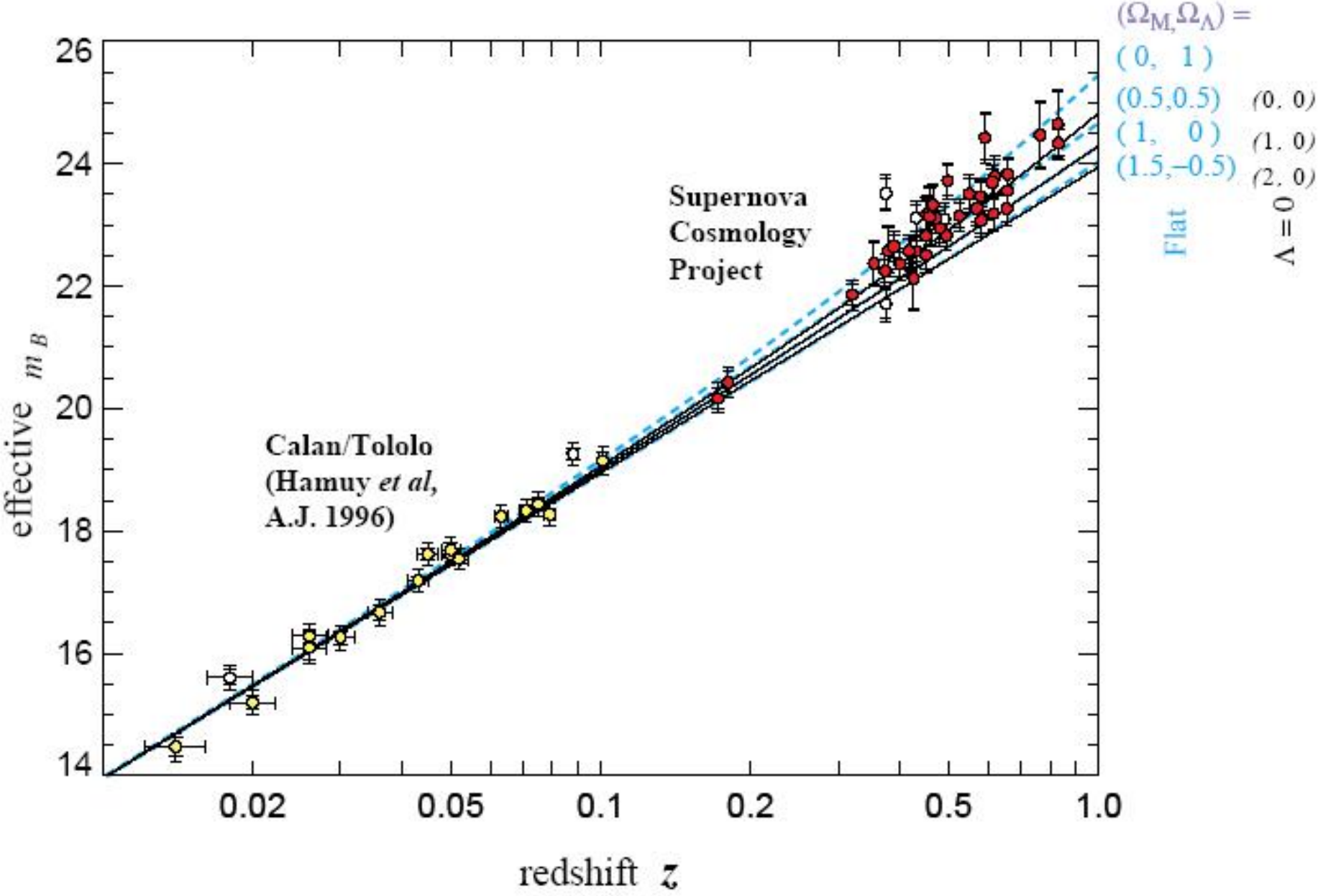
$(\Omega_M,\Omega_\Lambda)$ =
(0, 1)
(0.5,0.5)
(1, 0)
(1.5,–0.5)
(0, 0)
(1, 0)
(2, 0)
Flat
$\Lambda = 0$
Supernova
Cosmology
Project
Calan/Tololo
(Hamuy *et al*,
A.J. 1996)
effective m_B
redshift z
26
24
22
20
18
16
14
0.02
0.05
0.1
0.2
0.5
1.0

Measurements of Cosmic Microwave Background fluctuations

Satellites: Relikt, COBE, WMAP (2001), Planck (2006)

Baloons: Boomegang, Maxima, CBI, ACBAR, …

Hot Universe, flat model, Ω =1

Dark energy (Λ – term) Ω =0.7, Dark matter (nonbarionic) Ω =0.26, Baryonic Ω =0.04

Equilibrium Planck radiation with temperature about 3 K was left as a result of expansion of the hot universe (n, gravitons).

Matter had separated from the radiation at redshift **Z** about 1000. Radiation preserves non-uniformities of that period.

Study of CMB fluctuations permitted to evaluate the global parameters of the universe:

Ω and its ingradients, H – Hubble "constant", determining the rate of the universe expansion around us:

V=Hr, H~70 km/s/Mpc

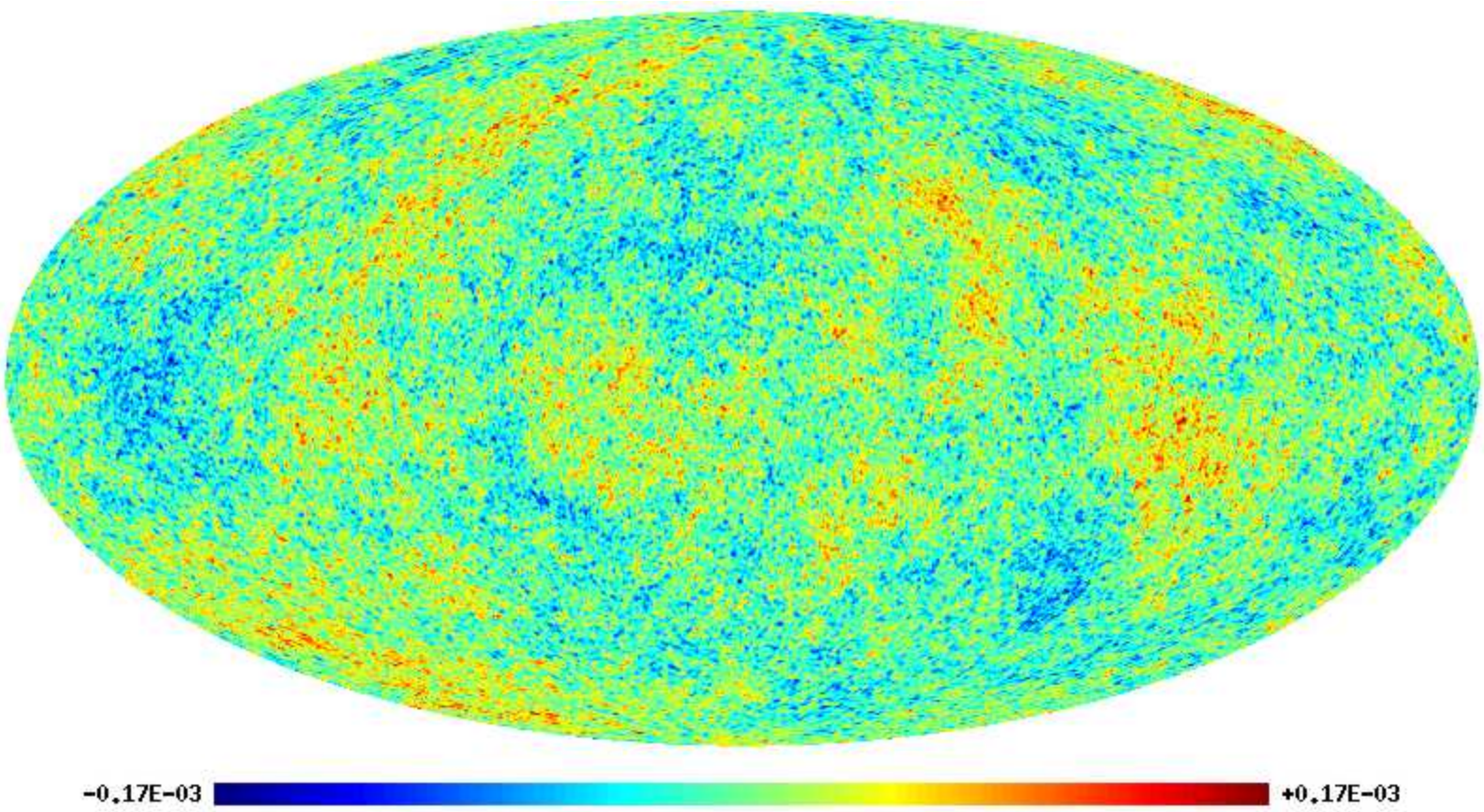

WMAP

M. Liguori et al., 2003

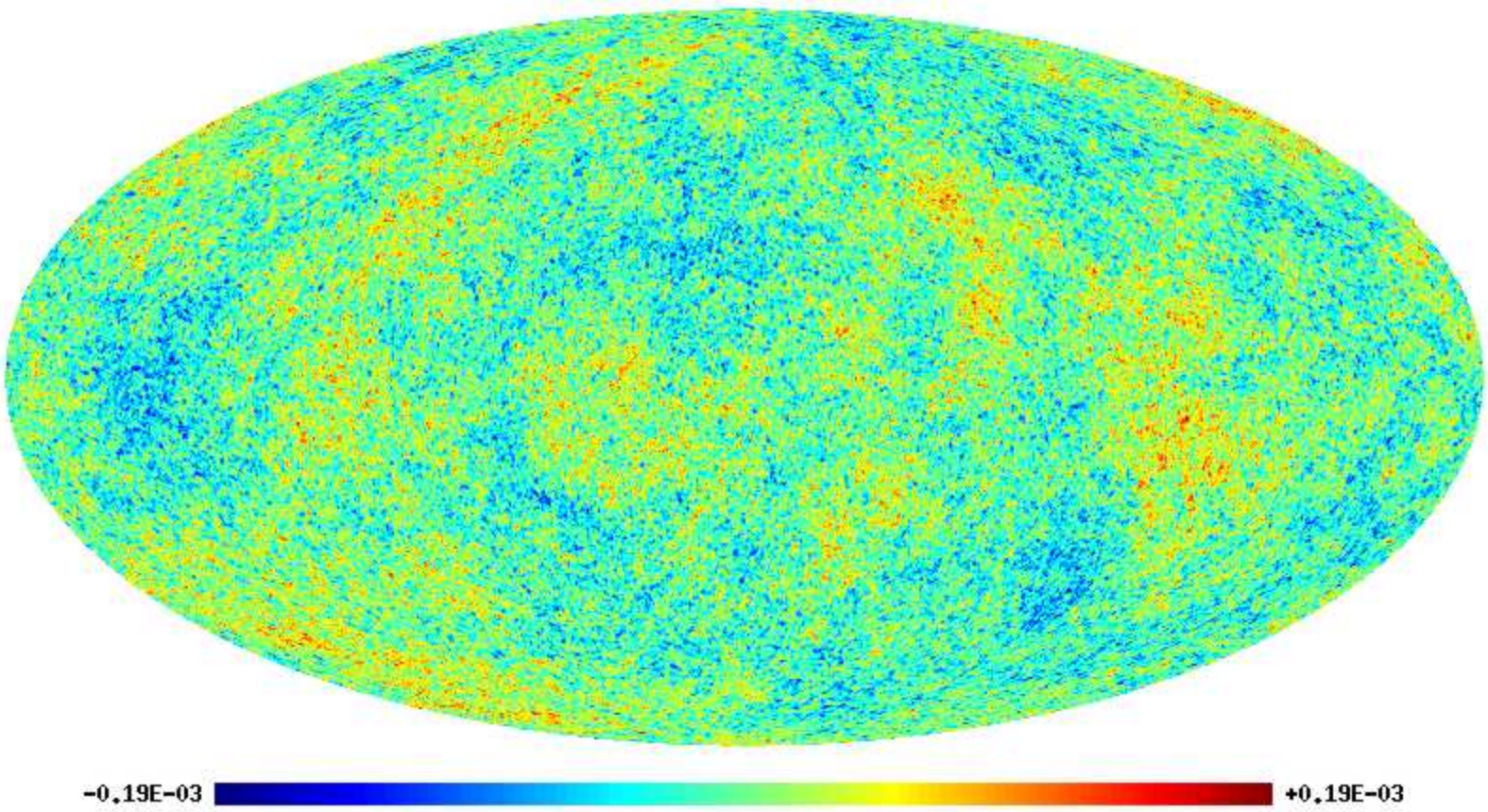

Planck (simulation)

M. Liguori et al., 2003

Planck 2013 results. XVI. Cosmological parameters

arXiv:1303.5076v1 [astro-ph.CO] 20 Mar 2013

	Planck+WP	*Planck*+WP+BAO	*WMAP*-9
$\Omega_b h^2$	0.02206 ± 0.00028	0.02220 ± 0.00025	0.02309 ± 0.00130
$\Omega_c h^2$	0.1174 ± 0.0030	0.1161 ± 0.0028	0.1148 ± 0.0048
τ	0.095 ± 0.014	0.097 ± 0.014	0.089 ± 0.014
H_0	65.2 ± 1.8	66.7 ± 1.1	73.9 ± 10.9
n_s	0.975 ± 0.012	0.969 ± 0.012	0.973 ± 0.014
$\log(10^{10} A_s)$	3.106 ± 0.029	3.100 ± 0.029	3.090 ± 0.039
α/α_0	0.9936 ± 0.0043	0.9989 ± 0.0037	1.008 ± 0.020

$$Y_P = 0.266 \pm 0.021 \quad (68\%;\ \textit{Planck}\text{+WP+highL}).$$

$$\sum m_\nu < \begin{cases} 0.98\,\text{eV} & (95\%;\ \textit{Planck}\text{+WP+highL}) \\ 0.32\,\text{eV} & (95\%;\ \textit{Planck}\text{+WP+highL+BAO}). \end{cases}$$

$$\Omega_\Lambda = 0.686 \pm 0.020 \quad (68\%;\ \textit{Planck}),$$

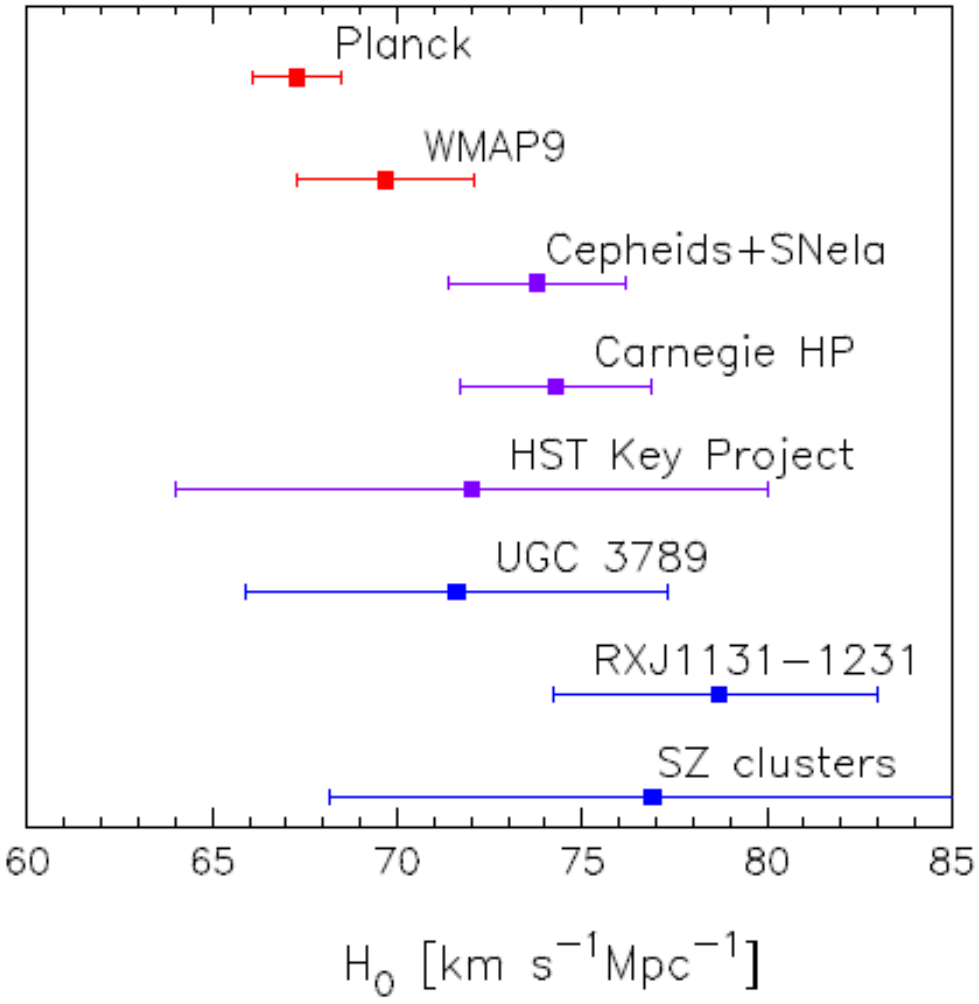

Fig. 16. Comparison of H_0 measurements, with estimates of $\pm 1\,\sigma$ errors, from a number of techniques (see text for details). These are compared with the spatially-flat ΛCDM model constraints from *Planck* and *WMAP*-9.

ArXiv 1312.3313

PLANCK DATA RECONSIDERED

David N. Spergel[1], Raphael Flauger[2,3] & Renée Hložek[1]

The tension between the best fit parameters derived by the Planck team and a number of other astronomical measurements suggests either systematics in the astronomical measurements, systematics in the Planck data, the need for new physics, or a combination thereof. We re-analyze the Planck data and find that the 217 GHz × 217 GHz detector set spectrum used in the Planck analysis is responsible for some of this tension. We use a map-based foreground cleaning procedure, relying on a combination of 353 GHz and 545 GHz maps to reduce residual foregrounds in the intermediate frequency maps used for cosmological inference. For our baseline data analysis, which uses 47% of the sky and makes use of both 353 and 545 GHz data for foreground cleaning, we find the ΛCDM cosmological parameters $\Omega_c h^2 = 0.1169 \pm 0.0025$, $n_s = 0.9671 \pm 0.0069$, $H_0 = 68.0 \pm 1.1\,\mathrm{km\ s^{-1}Mpc^{-1}}$, $\Omega_b h^2 = 0.02197 \pm 0.00027$, $\ln 10^{10} A_s = 3.080 \pm 0.025$, and $\tau = 0.089 \pm 0.013$. While in broad agreement with the results reported by the Planck team, these revised parameters imply a universe with a lower matter density of $\Omega_m = 0.302 \pm 0.015$, and parameter values generally more consistent with pre-Planck CMB analyses and astronomical observations. We compare our cleaning procedure with the foreground modeling used by the Planck

All perturbations are correlated, so to the moment of recombination amplitudes of harmonics oscillale – Doppler peaks (**Sakharov oscillations**)

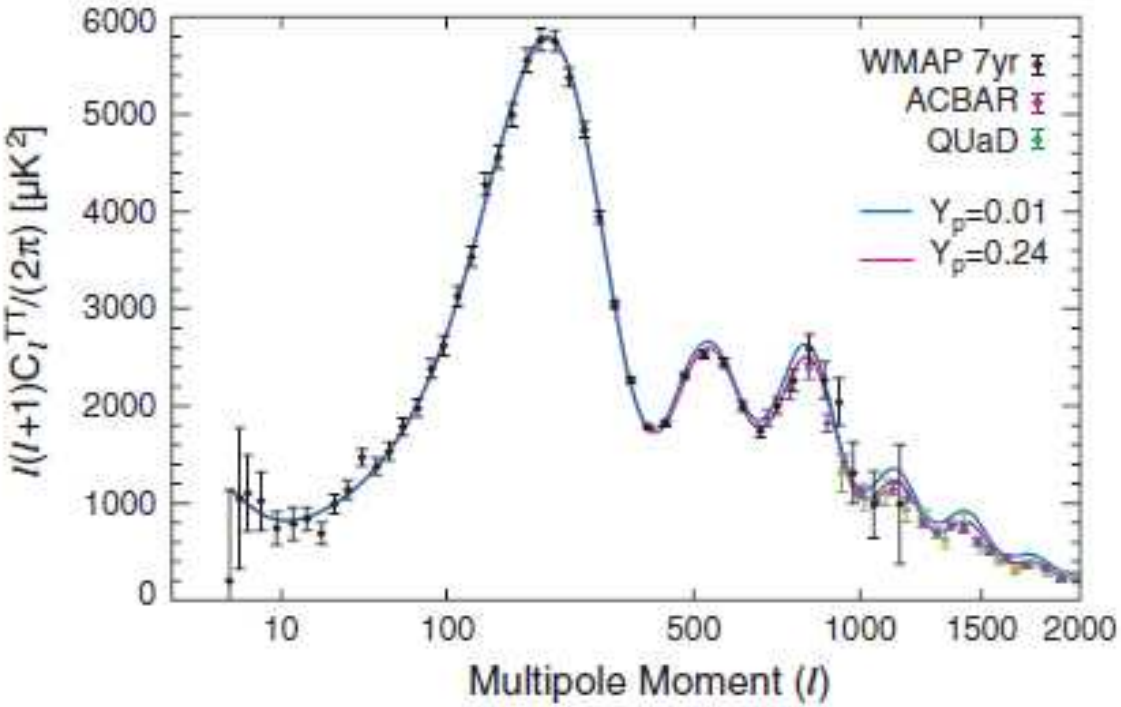

Figure 10. Primordial helium abundance and the temperature power spectrum. The data points are the same as those in Figure 7. The lower (pink) solid line (which is the same as the solid line in Figure 7) shows the power spectrum with the nominal helium abundance, $Y_p = 0.24$, while the upper (blue) solid line shows that with a tiny helium abundance, $Y_p = 0.01$. The larger the helium abundance is, the smaller the number density of electrons during recombination becomes, which enhances the Silk damping of the power spectrum on small angular scales, $l \gtrsim 500$.

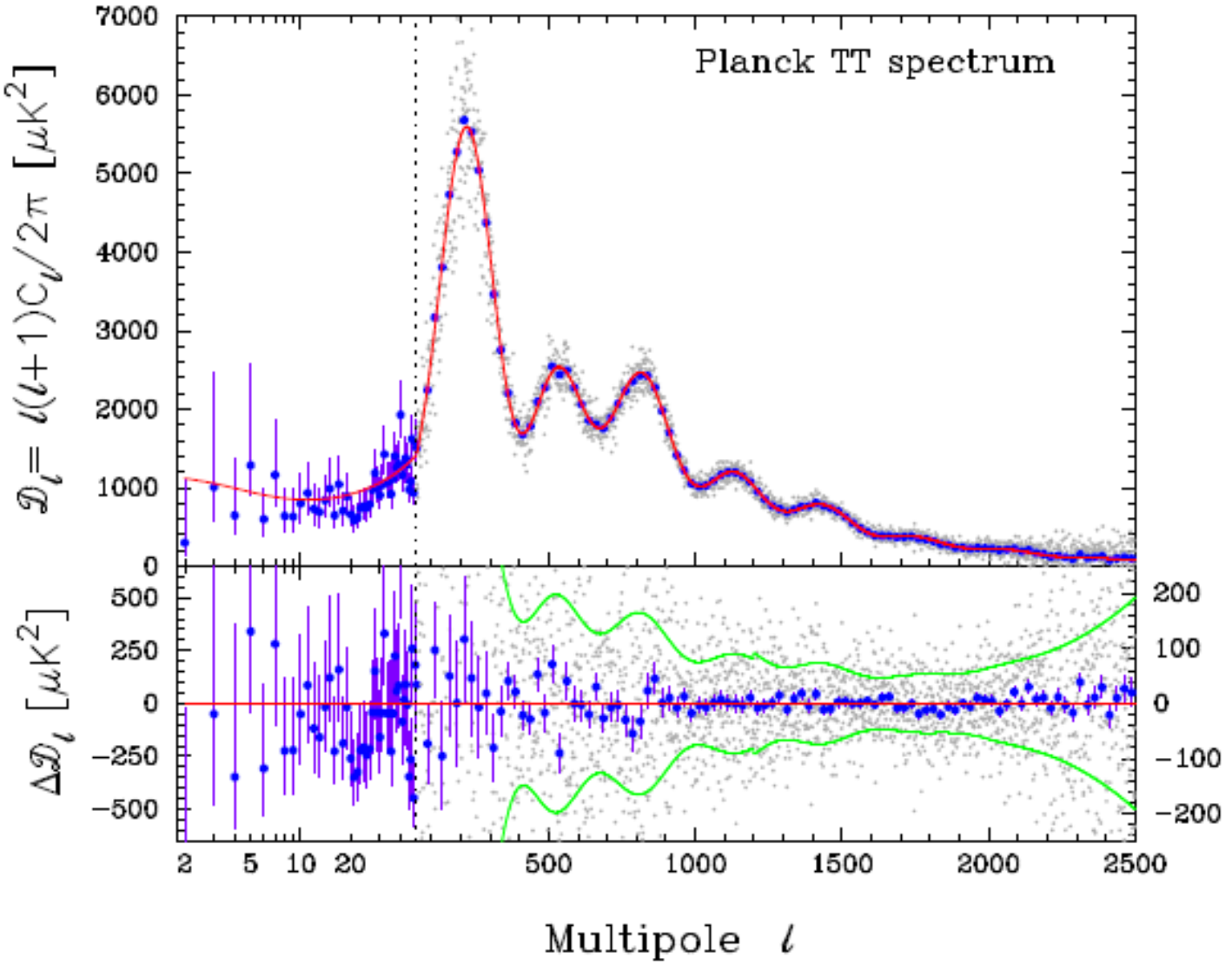
Planck TT spectrum
$\mathcal{D}_\ell = \ell(\ell+1)C_\ell/2\pi$ [μK^2]
$\Delta\mathcal{D}_\ell$ [μK^2]
Multipole ℓ
7000
6000
5000
4000
3000
2000
1000
0
500
250
0
−250
−500
200
100
0
−100
−200
2
5
10
20
500
1000
1500
2000
2500

In papers of **A. Chernin:, Physics-Uspekhi, 44, 1099 (2001), and Physics-Uspekhi, 51, 267 (2008),** the question was raised about a possible influence of DE on the properties of local universe

The importance of the DE for the structure of the local galaxy cluster (LC) depends on the level of the influence of DE on the dynamic properties. In particular, it is necessary to check, if the LC may exist in the equilibrium state, at present values of DE density, and the LC densities of matter, consisting of the baryonic, and dark matter (BM and DM).

Astrophys Space Sci (2012) 338:337–343

Dark energy and key physical parameters of clusters of galaxies

G.S. Bisnovatyi-Kogan · A.D. Chernin

We study physics of clusters of galaxies embedded in the cosmic dark energy background. Under the assumption that dark energy is described by the cosmological constant, we show that the dynamical effects of dark energy are strong in clusters like the Virgo cluster. Specifically, the key physical parameters of the dark mater halos in clusters are determined by dark energy:

(1) the halo cut-off radius is practically, if not exactly, equal to the zero-gravity radius at which the dark matter gravity is balanced by the dark energy antigravity;

(2) the halo averaged density is equal to two densities of dark energy;

(3) the halo edge (cut-off) density is the dark energy density with a numerical factor of the unity order slightly depending on the halo profile.

$$F(r) = F_N(r) + F_E(r) = -G\frac{M}{r^2} + \frac{8\pi G}{3}\rho_\Lambda r.$$

The total force *F* and the acceleration are both zero at the distance

$$r = R_\Lambda = \left[\frac{M}{\frac{8\pi}{3}\rho_\Lambda}\right]^{1/3}.$$

Here R_*lambda* is the zero-gravity radius

This radius is an absolute upper limit for the radial size *R* of a static cluster:

Taking for an estimate the total mass of the Virgo cluster (dark matter and baryons) M = (0.6–1.2) × 10^15 M_solar and the cosmological dark energy density ρ_v, one finds the zero-gravity radius of the Virgo cluster: R _*lambda*= (9–11) Mpc.

arXiv:1303.3800
A&A, Volume 553, id.A101, 4 pp (2013)

Dark energy and the structure of the Coma cluster of galaxies

A. D. Chernin, G.S. Bisnovatyi-Kogan, P. Teerikorpi,
M. J. Valtonen, G.G. Byrd, M. Merafina

R< 20 Mpc
M< 6.2 10^15 **M** Solar

arXiv:1303.7166
MNRAS, Volume 434, Issue 4, p.3628-3632 (2013)

Galactic cluster winds in presence of a dark energy

G.S. BISNOVATYI-KOGAN and M. MERAFINA

We obtain a solution for the hydrodynamic outflow of the polytropic gas from the gravitating center, in presence of the uniform Dark Energy (DE). The antigravity of DE is enlightening the outflow and make the outflow possible at smaller initial temperature, at the same density. The main property of the wind in presence of DE is its unlimited acceleration after passing the critical point. In application of this solution to the winds from galaxy clusters we suggest that collision of the strongly accelerated wind with another galaxy cluster, or with another galactic cluster wind could lead to the formation of a highest energy cosmic rays.

Subject headings: dark energy— galaxy clusters—galactic wind

EQUATIONS

$$\rho v\frac{dv}{dr}+\frac{dP}{dr}=-\rho\left(\frac{GM}{r^2}-\frac{\Lambda c^2 r}{3}\right)=-\rho\left(\frac{GM}{r^2}-\frac{8\pi G\rho_\Lambda r}{3}\right).$$

$$\Delta\Phi_\Lambda=-8\pi G\rho_\Lambda,\quad \Delta\Phi_g=4\pi G\rho,\quad \rho_\Lambda=\frac{\Lambda c^2}{8\pi G}.$$

$$4\pi\rho v r^2=\dot{M},$$

No self-gravity of the matter

$$P = K\rho^\gamma, \quad c_s^2 = \gamma\frac{P}{\rho}, \quad \rho = \left(\frac{c_s^2}{\gamma K}\right)^{\frac{1}{\gamma-1}}, \quad P = \left(\frac{c_s^2}{\gamma}\right)^{\frac{\gamma}{\gamma-1}} K^{-\frac{1}{\gamma-1}}$$

Introduce nondimensional variables as

$$\tilde{v} = \frac{v}{v_*} \quad \tilde{c}_s = \frac{c_s}{c_*}, \quad \tilde{r} = \frac{r}{r_*}, \quad r_* = \frac{GM}{c_*^2}, \quad v_* = c_*,$$

$$\tilde{\rho} = \frac{\rho}{\rho_*}, \quad \tilde{P} = \frac{P}{P_*}, \quad \rho_* = \left(\frac{c_*^2}{\gamma K}\right)^{\frac{1}{\gamma-1}}, \quad P_* = \left(\frac{c_*^2}{\gamma}\right)^{\frac{\gamma}{\gamma-1}} K^{-\frac{1}{\gamma-1}}.$$

$$\tilde{v}\frac{d\tilde{v}}{dr} + \frac{2}{\gamma-1}\tilde{c}_s\frac{d\tilde{c}_s}{d\tilde{r}} + \frac{1}{\tilde{r}^2} - \lambda\tilde{r} = 0, \quad \lambda = \frac{\Lambda c^2 r_*^2}{3c_*^2}.$$

$$\tilde{\rho}\,\tilde{v}\,\tilde{r}^2 = \dot{m}, \quad \tilde{c}_s^{\frac{2}{\gamma-1}}\tilde{v}\tilde{r}^2 = \dot{m}, \quad \dot{m} = \frac{\dot{M}}{\dot{M}_*}, \quad \dot{M}_* = 4\pi\rho_* v_* r_*^2.$$

$$\frac{d\tilde{\rho}}{\tilde{\rho}} = \frac{2}{\gamma - 1}\frac{d\tilde{c}_s}{\tilde{c}_s}, \quad \frac{d\tilde{\rho}}{\tilde{\rho}} + \frac{d\tilde{v}}{\tilde{v}} + 2\frac{d\tilde{r}}{\tilde{r}} = 0.$$

$$\frac{d\tilde{v}}{d\tilde{r}} = \frac{\tilde{v}}{\tilde{r}} \frac{2\tilde{c}_s^2 - \frac{1}{\tilde{r}} + \lambda\tilde{r}^2}{\tilde{v}^2 - \tilde{c}_s^2}.$$

$$\tilde{v} = \tilde{c}_s, \quad 2\tilde{c}_s^2 - \frac{1}{\tilde{r}} + \lambda\tilde{r}^2 = 0$$

Singular point

Choosing $c_* = c_{sc}$, we obtain in the critical point

$$\tilde{v}_c = \tilde{c}_{sc} = 1, \quad 2 - \frac{1}{\tilde{r}_c} + \lambda\tilde{r}_c^2 = 0.$$

$$\dot{m} = \tilde{r}_c^2.$$

$$\frac{\tilde{v}^2}{2}+\frac{\tilde{c}_s^2}{\gamma-1}-\frac{1}{\tilde{r}}-\frac{\lambda\tilde{r}^2}{2}=h,\quad \tilde{c}_s^2=\left(\frac{\dot{m}}{\tilde{v}\tilde{r}^2}\right)^{\gamma-1}=\left(\frac{\tilde{r}_c^2}{\tilde{v}\tilde{r}^2}\right)^{\gamma-1}.$$

Bernoulli integral

$$h=\frac{\gamma+1}{2(\gamma-1)}-\frac{1}{\tilde{r}_c}-\frac{\lambda\tilde{r}_c^2}{2}=\frac{5-3\gamma}{2(\gamma-1)}-\frac{3}{2}\left(\frac{1}{\tilde{r}_c}-2\right).$$

Without DE

$$\tilde{r}_c=\frac{1}{2},\quad h=\frac{5-3\gamma}{2(\gamma-1)}.$$

DE mass inside the critical radius is does not exceed the gravity of the central body at

$$\lambda < \frac{16\pi^2}{9} = 17.55 = \lambda_{lim}.$$

Effective grav. potential (DE+matter)

$$\tilde{\Phi} = -\frac{1}{\tilde{r}} - \frac{\lambda \tilde{r}^2}{2}.$$

$$h \geq \tilde{\Phi}_{max}(\tilde{r}_{max}) = -\frac{3}{2}\lambda^{1/3}, \quad \tilde{r}_{max} = \lambda^{-1/3}.$$

To penetrate the potential barrier – possible at negative h in presence of DE.

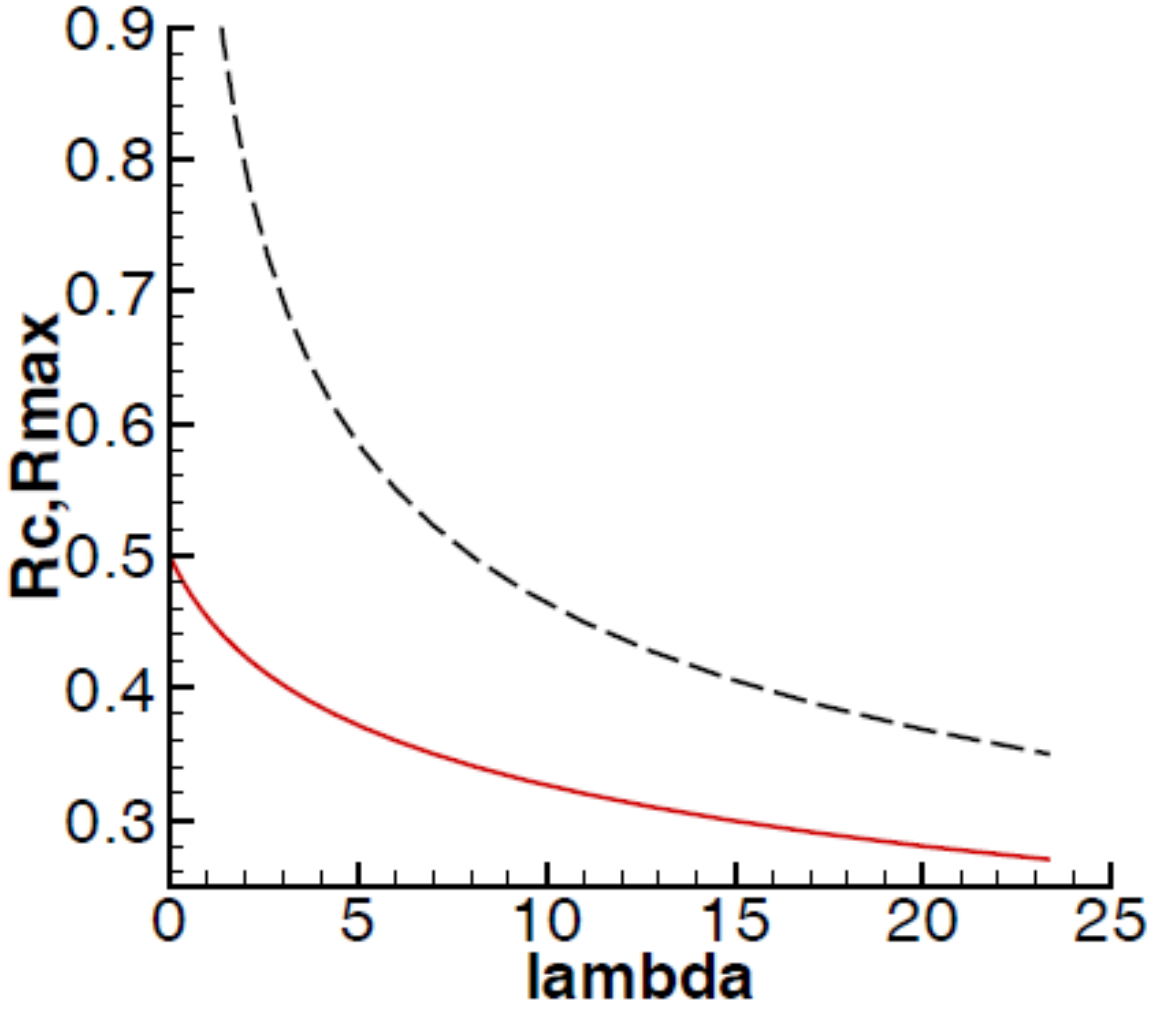

Fig. 1.— The functions $\tilde{r}_c(\lambda)$ (full curve), according to (12), and $\tilde{r}_{max}(\lambda)$ (dashed curve) according to (22). It is clear, that the critical radius of the flow r_c is always inside the radius of the extremum of the total gravitational potential r_{max}.

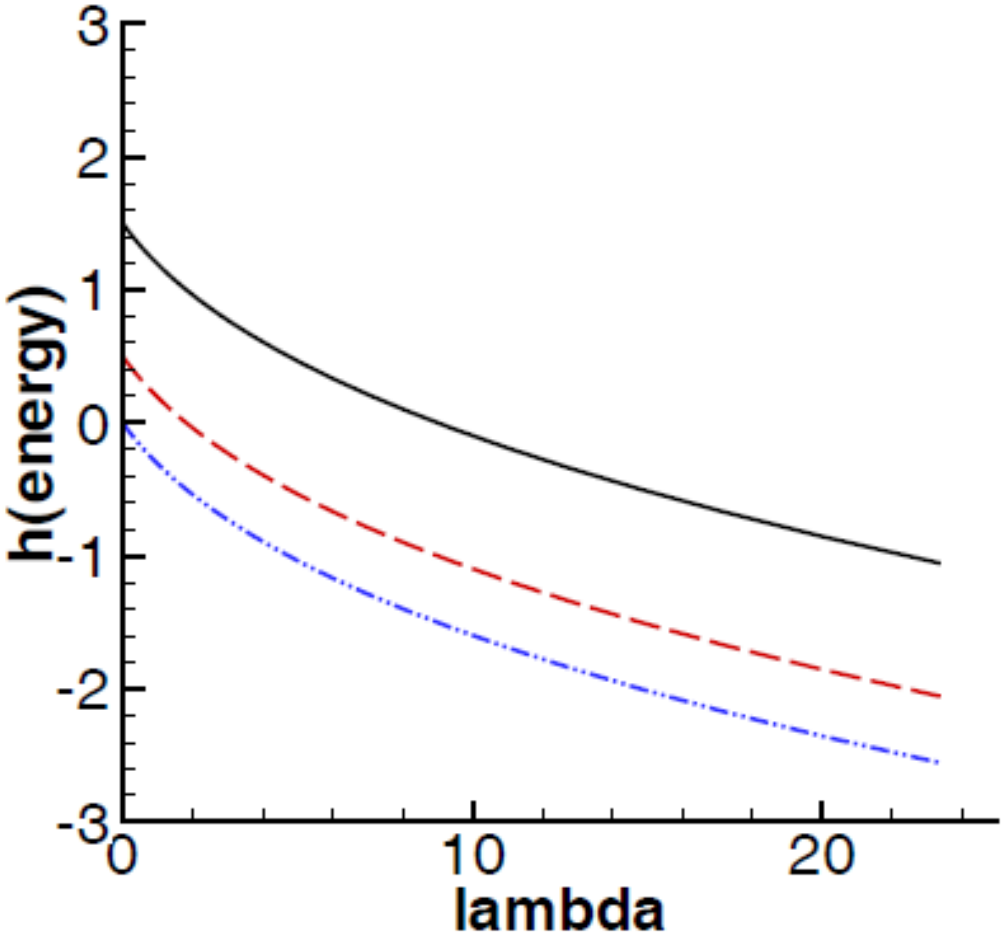

Fig. 2.— The function $h(\lambda)$ for $\gamma = \frac{4}{3}$ (full curve); $\gamma = \frac{3}{2}$ (dashed curve); $\gamma = \frac{5}{3}$ (dash-dot-dot curve), according to relations (12),(15).

Analytical solutions exist only in absence of DE, $\Lambda = 0$.

$$\tilde{r}_c = \frac{1}{2}, \quad h = \frac{\tilde{v}^2}{2} + \frac{\tilde{c}_s^2}{\gamma - 1} - \frac{1}{\tilde{r}} = \frac{5 - 3\gamma}{2(\gamma - 1)}.$$

At $h = 0$ and $\gamma = \frac{5}{3}$:

$$H = \frac{v^2}{2} + \frac{3c_s^2}{2} - \frac{GM}{r} = 0.$$

Exact solution with any constant Mach number

$$v^2 = \frac{2GM}{r}\frac{\mathrm{Ma}^2}{3 + \mathrm{Ma}^2}, \qquad c_s^2 = \frac{2GM}{r}\frac{1}{3 + \mathrm{Ma}^2}.$$

$$\gamma = 1.5,$$
$$h = 0.5.$$
$$r_c = 0.5,$$

$$\tilde{c}_s^2 = \left(\frac{\tilde{r}_c^2}{\tilde{v}\tilde{r}^2}\right)^{\gamma-1} = \sqrt{\frac{1}{4\tilde{v}\tilde{r}^2}},$$

$$\mathbf{1}.\ \tilde{v} = 1; \qquad \mathbf{2}.\ \tilde{r} = \frac{2}{\sqrt{\tilde{v}}(1+\sqrt{\tilde{v}})(1+\tilde{v})}.$$

wind

accretion

Numerical solutions

To obtain a physically relevant critical solution of (10), with $\tilde{c}_s^2$ from (14), we obtain expansion in the critical point with $\tilde{v}^2 = \tilde{c}_s^2 = 1$, in the form

$$\tilde{v} = 1 + \alpha(\tilde{r} - \tilde{r}_c), \quad \alpha_1 = -\frac{2}{\tilde{r}_c}\frac{\gamma-1}{\gamma+1} + \frac{1}{\tilde{r}_c}\frac{2}{\gamma+1}\sqrt{2 + \frac{1}{4\tilde{r}_c} + \frac{\lambda\tilde{r}_c^2}{2} - \gamma\left(2 - \frac{1}{4\tilde{r}_c} - \frac{\lambda\tilde{r}_c^2}{2}\right)},$$

wind

$$\alpha_2 = -\frac{2}{\tilde{r}_c}\frac{\gamma-1}{\gamma+1} - \frac{1}{\tilde{r}_c}\frac{2}{\gamma+1}\sqrt{2 + \frac{1}{4\tilde{r}_c} + \frac{\lambda\tilde{r}_c^2}{2} - \gamma\left(2 - \frac{1}{4\tilde{r}_c} - \frac{\lambda\tilde{r}_c^2}{2}\right)}.$$

accretion

Without DE

$$\alpha_1 = \frac{4}{\gamma+1}\left[\sqrt{\frac{5-3\gamma}{2}} - (\gamma-1)\right],$$

$$\alpha_2 = -\frac{4}{\gamma+1}\left[\sqrt{\frac{5-3\gamma}{2}} + (\gamma-1)\right].$$

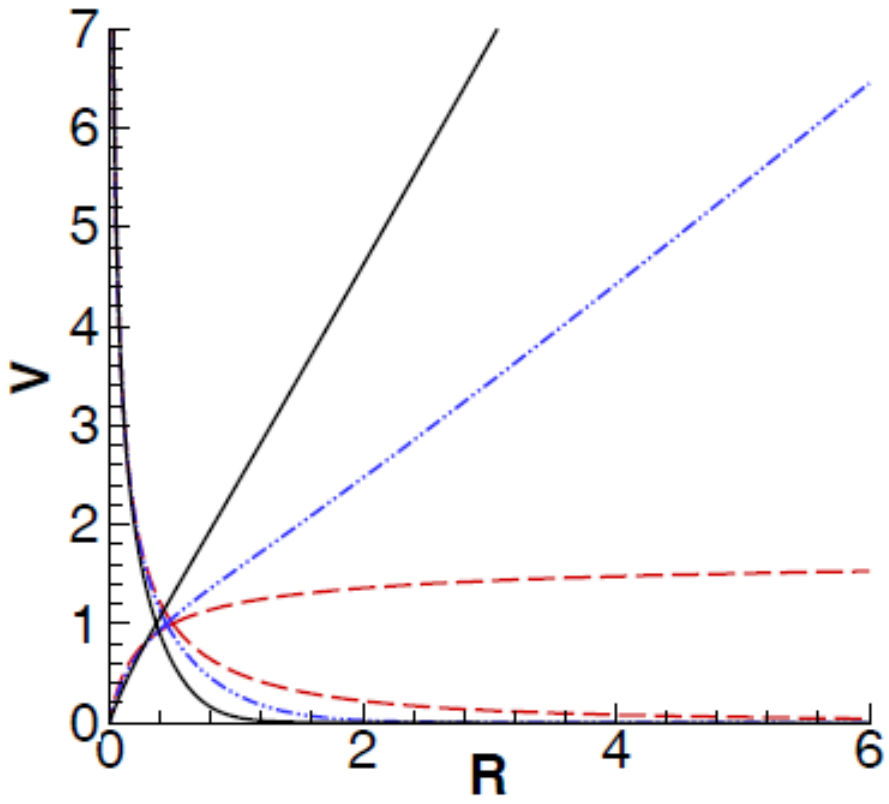

Fig. 4.— The integral curves of the equations (10), (14), for $\gamma = 4/3$ and $\lambda = 0$, r_c=0.5 (dashed curves); $\lambda = 1.10$, $r_c = 0.45$ (dash-dot-dot curves); and $\lambda = 5.13$, $r_c = 0.37$ (full curves). Wind solutions correspond to curves with increasing velocity at large radius. The curves with decreasing velocities correspond to the accretion solution with negative v, so that its absolute value is presented.

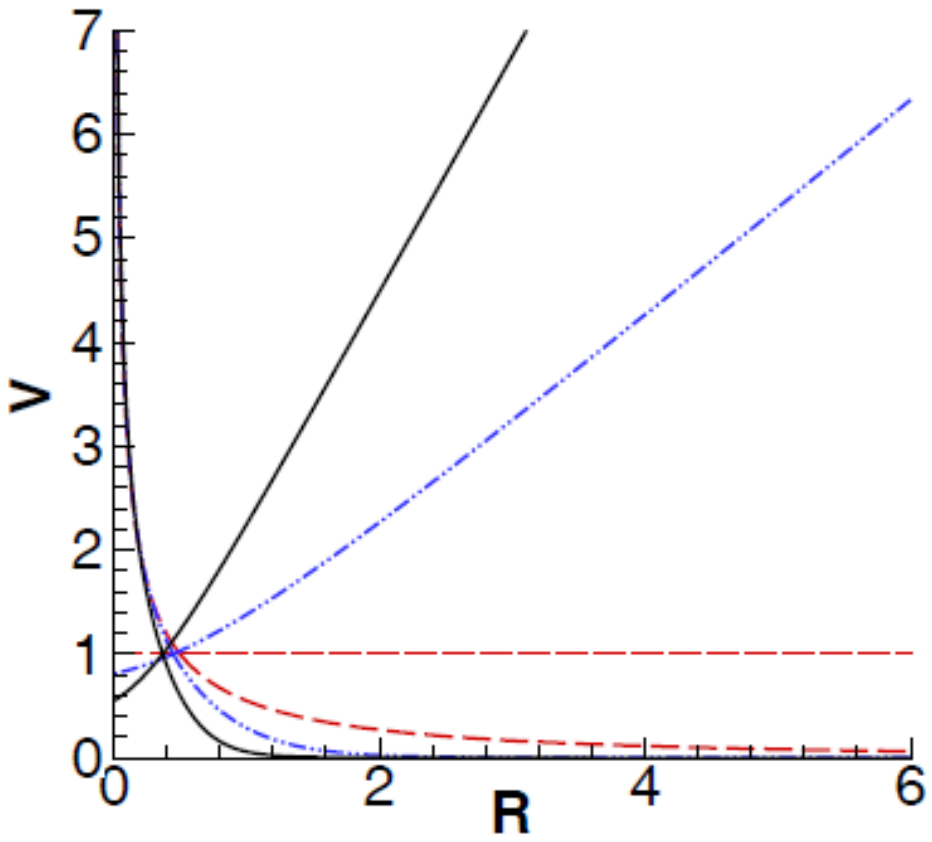

Fig. 5.— The integral curves of the equations (10), (14), for $\gamma = 3/2$ and $\lambda = 0$, r_c=0.5 (dashed curves); $\lambda = 1.10$, $r_c = 0.45$ (dash-dot-dot curves); and $\lambda = 5.13$, $r_c = 0.37$ (full curves). Wind solutions correspond to curves with increasing (or constant) velocity at large radius. The curves with decreasing velocities correspond to the accretion solution with negative v, so that its absolute value is presented.

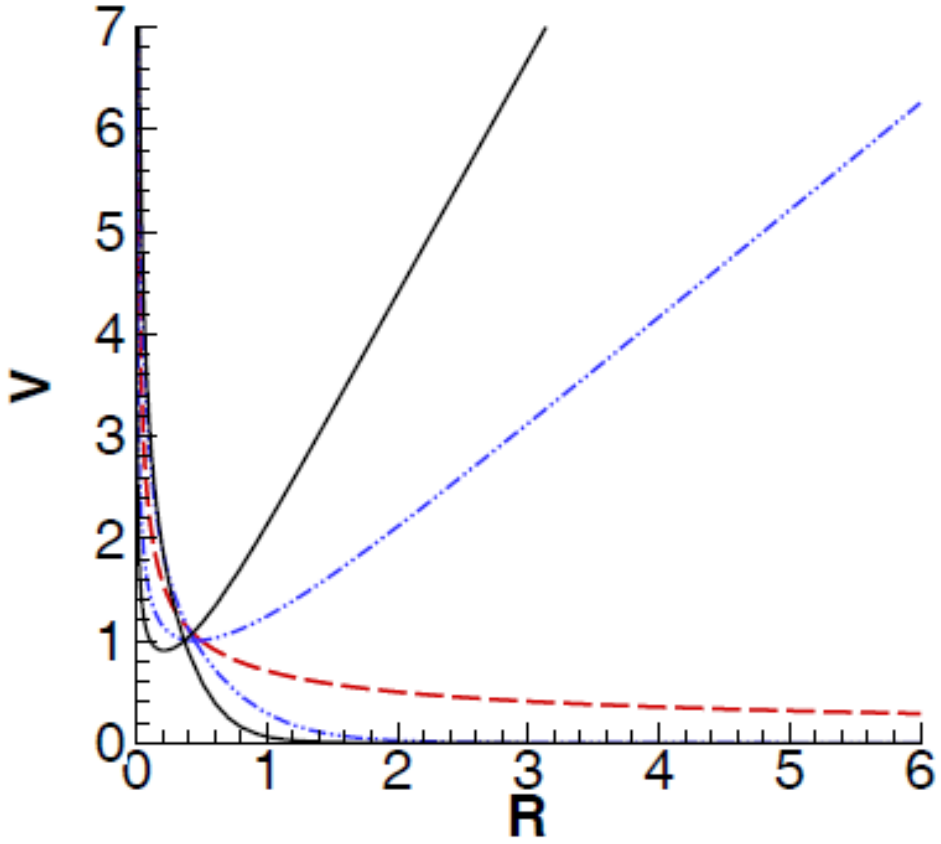

Fig. 6.— The integral curves of the equations (10), (14), for $\gamma = 5/3$ and $\lambda = 0$, r_c=0.5 (dashed curve); $\lambda = 1.10$, $r_c = 0.45$ (dash-dot-dot curves); and $\lambda = 5.13$, $r_c = 0.37$ (full curves). For nonzero λ wind solutions correspond to curves with increasing velocity at large radius. The curves with decreasing velocities correspond to the accretion solution with negative v, so that its absolute values are presented. At $\lambda = 0$ both wind and accretion solutions are presented by the same curve, which corresponds to the wind for positive v, and to the accretion for negative v.

Let us consider outer parts of the Coma cluster at radius $R_C = 15$ Mpc, with the mass inside $M_C = 5 \cdot 10^{15}\, M_\odot$, from Chernin et al. (2013). For the present value of $\rho_\Lambda = 0.71 \cdot 10^{-29}$ g/cm^3, supposing that $R_C = r_*$ is the critical radius of the wind, we obtain from (2),(7), the nondimensional constant λ as

$$\lambda = \frac{\Lambda c^2 r_*^2}{3 c_*^2} = \frac{8\pi}{3}\frac{\rho_\Lambda r_*^3}{M} \approx 0.59, \quad c_* = \sqrt{\frac{G\,M_C}{R_C}} \approx 1200 \text{ km/c}.$$

It corresponds to the temperature about $T \approx 6 \cdot 10^7$ K, $kT \approx 5$ keV. Observations of the hot gas distribution in the Coma cluster (Watanabe et al., 1999) on ASCA satellite have shown a presence of hot region with $kT = 11 - 14$ keV, and more extended cool region with $kT = 5 \pm 1$ keV, what is in good accordance with our choice of parameters.

Wind solutions for λ=0; 0.58; 1.1 are presented in Fig.7. The density of the gas in the vicinity of $r = r_c$ is very small, so the flow may be considered as adiabatic (polytropic) with the power γ=5/3. Without DE such gas flow is inefficient, its velocity is decreasing $\sim 1/\sqrt{r}$, see Eq. (25). In presence of DE the wind velocity is increasing 2 times at the distance of $\sim 5r_c \sim 75$ Mpc from Coma.

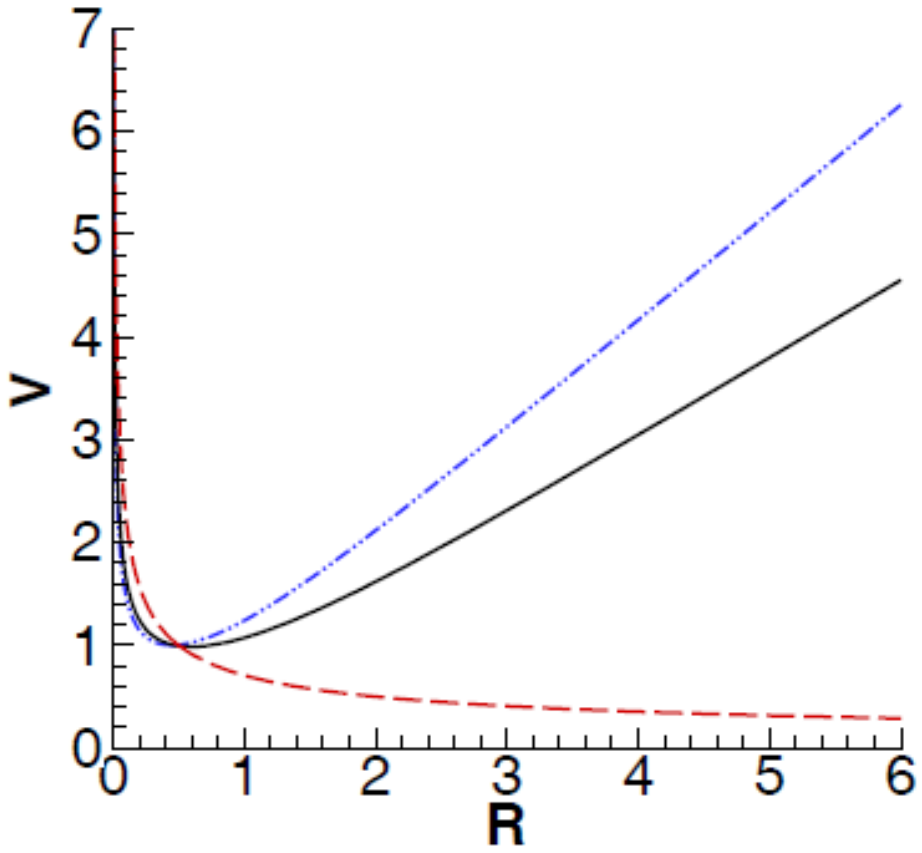

Fig. 7.— The integral curves of the equations (10), (14) for the wind solution, at $\gamma = 5/3$ and $\lambda = 0$, r_c=0.5 (dashed curve); $\lambda = 1.10$, $r_c = 0.45$ (dash-dot-dot curves); and $\lambda = 0.58$, $r_c = 0.47$ (full curves).

After quitting the cluster the gas is moving with acceleration, acting as a snow-plough for the intergalactic gas. The shell of matter, forming in such a way, may reach a high velocity, exceeding considerably the speed of galaxies in cluster. If the shell meets another cluster, or another shell moving towards, the collision of such flows may induce a particle acceleration. Due to high speed, large sizes, and low density such collisions may create cosmic rays of the highest possible energy (EHECR). We may expect the largest effect when two clusters move to each other. The influence of DE is decreasing with with a red shift, therefore the acceleration of EHECR in this model should take place in the periphery, or between, the closest rich galaxy clusters.

arXiv:astro-ph/0608407 v1 19 Aug 2006

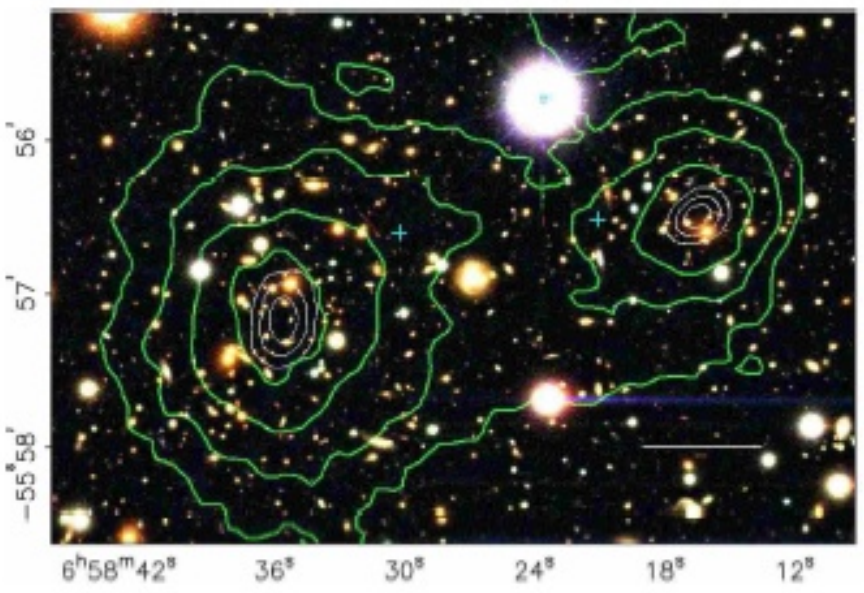

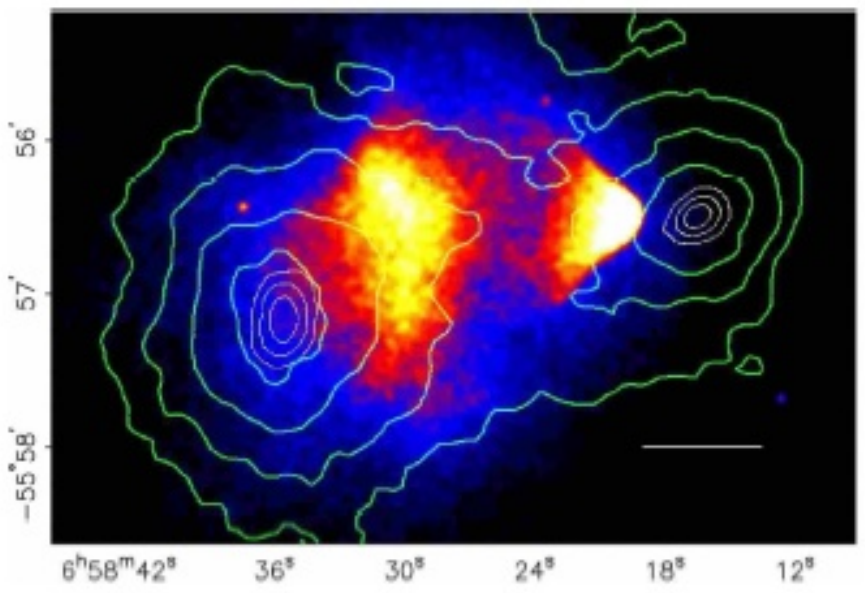

Left panel is a color image from the Magellan images of the merging cluster 1E0657−558, with the white bar indicating 200 kpc at the distance of the cluster. Right panel is a 500 ks Chandra image of the cluster. Shown in green contours in both panels are the weak lensing reconstruction with the outer contour level at = 0.16 and increasing in steps of 0.07. The white contours show the errors on the positions of the peaks and correspond to 68.3%, 95.5%, and 99.7% confidence levels. The blue +s show the location of the centers used to measure the masses of the plasma clouds

May be two colliding winds

Eichler, Usov, 1993

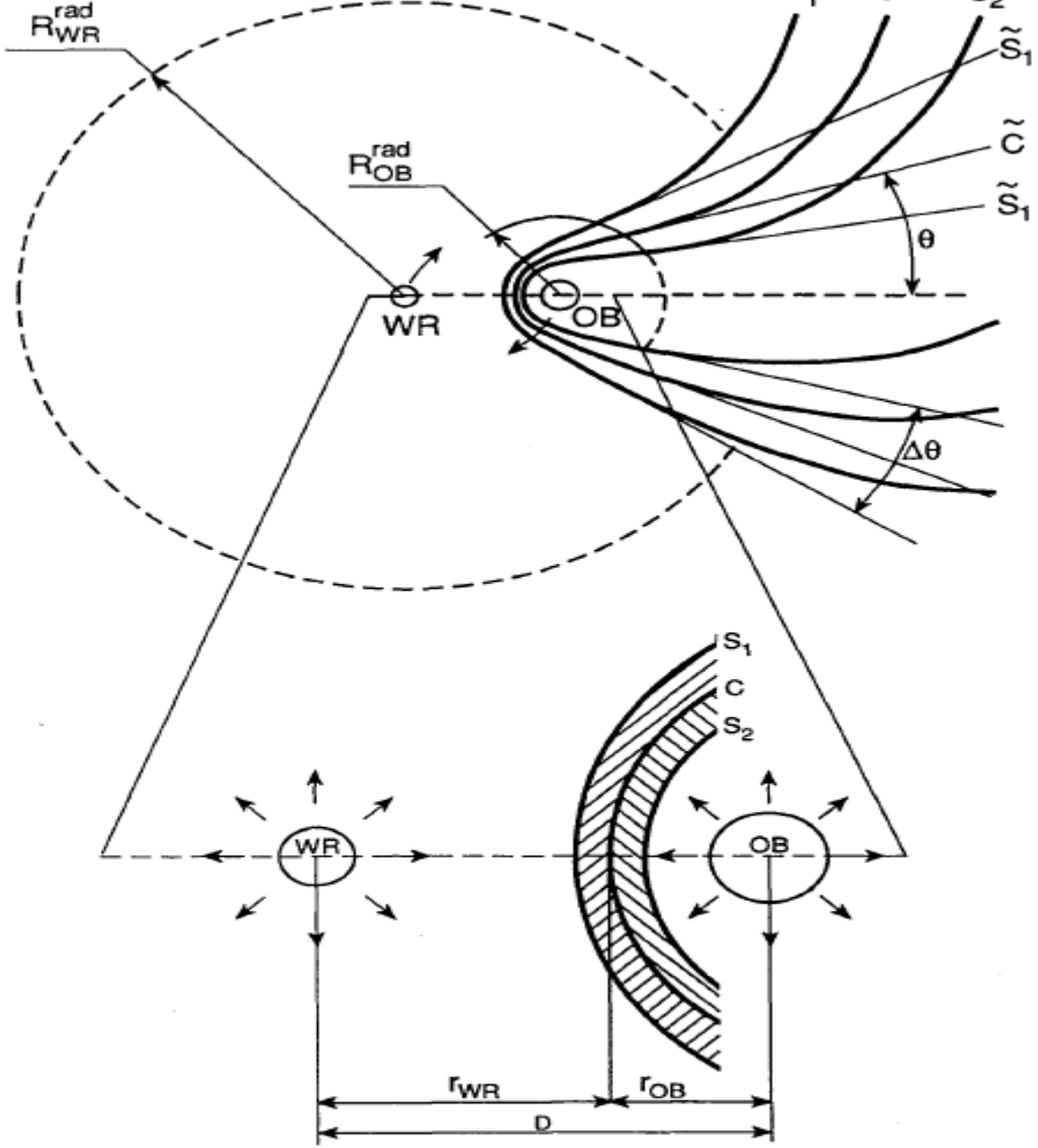

FIG. 1.—Collision of two stellar winds in the WR + OB binary. S_1 and S_2 denote the shock waves and C is the contact surface. The surfaces S_1, S_2, and C are near the conic surfaces $\tilde{S}_1$, $\tilde{S}_2$, and $\tilde{C}$, respectively, at intermediate distances

Greisen–Zatsepin–Kuzmin limit (1966)

Interactions between cosmic rays and the photons of the cosmic microwave background radiation (CMB)

Cosmic rays with energies over the threshold energy of 5×10^{19} eV would interact with cosmic microwave background photons

$$\gamma_{\mathrm{CMB}} + p \rightarrow \Delta^{+} \rightarrow p + \pi^{0},$$

or

$$\gamma_{\mathrm{CMB}} + p \rightarrow \Delta^{+} \rightarrow n + \pi^{+}.$$

Due to the mean path associated with this interaction, extragalactic cosmic rays traveling over distances larger than 50 Mpc (163 Mly) and with energies greater than this threshold should never be observed on Earth. This distance is also known as GZK horizon.

Cosmic Ray Spectra of Various Experiments

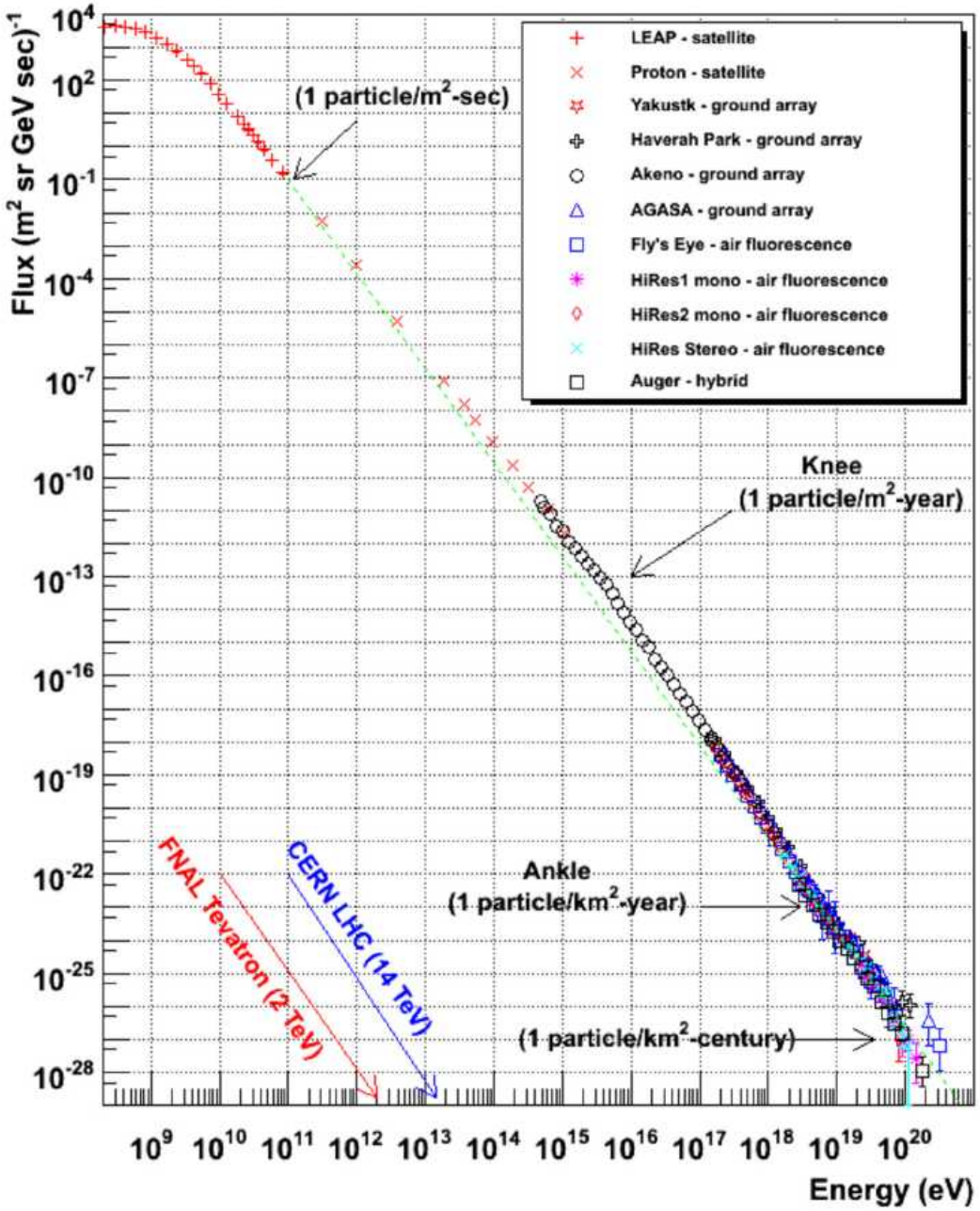

Nearby Galaxy clusters

Virgo galaxy cluster d= 17 Mpc

Coma galaxy Cluster d=100 Mpc

Hercules Galaxy Cluster (Abell 2151)
Distance: 500 Million Light Years = 170 Mpc

Conclusions

The density of DE, measured from SN Ia distributions, and spectra of fluctuations CMB perturbations, imply the necessity to take it into account in calculations of the structure of galaxy clusters.

The existing observational indefiniteness in the parameters of LC indicate to the dynamic importance of DE in the scale of the galaxy clusters.

Hot gas in GC is accelerated in presence of DE, and EHECR may be accelerated in rapid colliding winds from clusters, moving to each other